JACS
JOURNAL OF THE AMERICAN CHEMICAL SOCIETY

ARTICLE

pubs.acs.org/JACS

Characterization of Photoinduced Self-Exchange Reactions at Molecule−Semiconductor Interfaces by Transient Polarization Spectroscopy: Lateral Intermolecular Energy and Hole Transfer across Sensitized TiO_2 Thin Films

Shane Ardo and Gerald J. Meyer*

Departments of Chemistry and Materials Science and Engineering, Johns Hopkins University, 3400 North Charles Street, Baltimore, Maryland 21218, United States

Supporting Information

ABSTRACT: Transient anisotropy measurements are reported as a new spectroscopic tool for mechanistic characterization of photoinduced charge-transfer and energy-transfer self-exchange reactions at molecule−semiconductor interfaces. An anisotropic molecular subpopulation was generated by photoselection of randomly oriented Ru(II)−polypyridyl compounds, anchored to mesoscopic nanocrystalline TiO_2 or ZrO_2 thin films, with linearly polarized light. Subsequent characterization of the photoinduced dichromism change by visible absorption and photoluminescence spectroscopies on the nano- to millisecond time scale enabled the direct comparison of competitive processes: excited-state decay vs self-exchange energy transfer, or interfacial charge recombination vs self-exchange hole transfer. Self-exchange energy transfer was found to be many orders-of-magnitude faster than hole transfer at the sensitized TiO_2 interfaces; for $[Ru(dtb)_2(dcb)](PF_6)_2$, where dtb is 4,4′-$(C(CH_3)_3)_2$-2,2′-bipyridine and dcb is 4,4′-$(COOH)_2$-2,2′-bipyridine, anchored to TiO_2, the energy-transfer correlation time was θ_{ent} = 3.3 μs while the average hole-transfer correlation time was $\langle\theta_{h+}\rangle$ = 110 ms, under identical experimental conditions. Monte Carlo simulations successfully modeled the anisotropy decays associated with lateral energy transfer. These mesoscopic, nanocrystalline TiO_2 thin films developed for regenerative solar cells thus function as active "antennae", harvesting sunlight and transferring energy across their surface. For the dicationic sensitizer, $[Ru(dtb)_2(dcb)](PF_6)_2$, anisotropy changes indicative of self-exchange hole transfer were observed only when ions were present in the acetonitrile solution. In contrast, evidence for lateral hole transfer was observed in neat acetonitrile for a neutral sensitizer, *cis*-$Ru(dnb)(dcb)(NCS)_2$, where dnb is 4,4′-$(CH_3(CH_2)_8)_2$-2,2′-bipyridine, anchored to TiO_2. The results indicate that mechanistic models of interfacial charge recombination between electrons in TiO_2 and oxidized sensitizers must take into account diffusion of the injected electron *and* the oxidized sensitizer. The phenomena presented herein represent two means of concentrating potential energy derived from visible light that could be used to funnel energy to molecular catalysts for multiple-charge-transfer reactions, such as the generation of solar fuels.

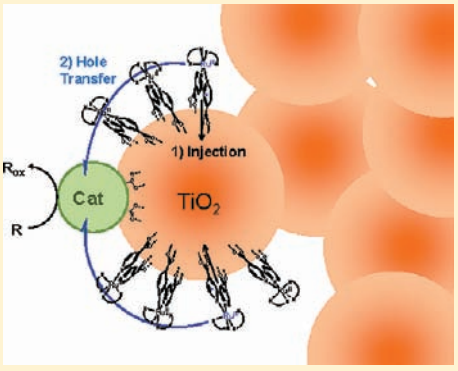

INTRODUCTION

Outer-sphere electron and energy self-exchange represent a simple class of reactions in which no bonds are broken and no bonds are formed, eqs 1 and 2, respectively, where bpy is 2,2′-bipyridine.

$$Ru(bpy)_3^{2+} + Ru(bpy)_3^{3+} \rightarrow Ru(bpy)_3^{3+} + Ru(bpy)_3^{2+} \quad (1)$$

$$Ru(bpy)_3^{2+*} + Ru(bpy)_3^{2+} \rightarrow Ru(bpy)_3^{2+} + Ru(bpy)_3^{2+*} \quad (2)$$

The equivalence of the reactants and products simplifies theoretical expressions and has enabled critical analysis of experimental data from which deep insights into the intrinsic reaction barriers have been garnered.[1,2] Self-exchange reactions are also of interest in natural and artificial photosynthesis, as they provide a general mechanism by which energy or charge can be transferred between molecules without the loss of free energy.[1,2] For example, in photosynthetic light harvesting antennae systems, chlorophyll*-to-chlorophyll energy transfer can rapidly and quantitatively deliver energy to a reaction center,[3] behavior that arises from a recently observed quantum coherent energy-transfer mechanism wherein nearly perfect excited-state alignment and environmental screening inhibit collisional decoherence.[4] Self-exchange energy transfer has also been observed in artificial photosynthetic assemblies like those based on the dye-sensitized, mesoscopic nanocrystalline TiO_2 thin films developed by Grätzel and co-workers for

Received: February 3, 2011
Published: August 23, 2011

application in regenerative photoelectrochemical cells.[5−8] Interestingly, lateral intermolecular self-exchange electron transfer, like that in eq 1, can also be induced in these same materials with an electrochemical bias.[9−13]

Historically, such self-exchange reactions have been difficult to quantify experimentally in heterogeneous materials due to the equivalence of reactants and products.[1] Conventional line-broadening measurements are nontrivial and complicated by interfacial heterogeneity that can in itself result in significant spectral broadening.[1,2] Such heterogeneity may induce a distribution of environments such that the reactants and products are not truly identical. It is therefore a simplification to consider eqs 1 and 2 as self-exchange processes in photosynthetic assemblies where aggregation, partial solvation, and other environmental factors may alter the reaction chemistry. Nevertheless, there still exists a real need to quantify interfacial "self-exchange reactions" that may be utilized for solar energy conversion and to provide fundamental insights into interfacial chemistry. For example, in dye-sensitized solar cells, one might want to know whether an oxidized dye molecule formed after excited-state injection stays localized on the injecting dye or hops to its neighbor or to a catalytic site. The extent to which lateral photoinduced self-exchange occurs at *any* semiconductor surface remains largely unknown. Given this impetus, we report herein transient anisotropy measurements[14,15] as a new spectroscopic assay for mechanistic characterization of photoinduced charge-transfer and energy-transfer self-exchange reactions at molecule−semiconductor interfaces.

The anisotropy assay can be understood with the aid of the idealized TiO_2 nanocrystallite with surface-anchored Ru(II)−polypyridyl compounds, shown in Scheme 1, where each compound's lowest-energy charge-transfer transition dipole moment is depicted by a singly degenerate, vectorial transition (blue arrow). An anisotropic molecular subpopulation can be generated by photoselection of these randomly oriented compounds with linearly polarized light excitation. The magnitude of the overlap between the molecular transition dipole moments and the polarization vector of the excitation light (polarized vertically and propagating in the plane of the page) is depicted as thick brown arrows, where ε is the absorption coefficient measured in isotropic fluid solution. This illustrates that compounds positioned closer to the vertical poles of a nanocrystallite will be preferentially photoexcited by the incoming vertically polarized light relative to those near the equator. For anchored molecules on immobilized nanoparticles, like those sintered together in the mesoporous thin films employed here, the direction of the photoselected transition dipole moments will move little due to molecular or nanoparticle diffusion; however, when molecules participate in lateral intermolecular energy- or hole-transfer reactions, the detected transition dipole moments will change. With pulsed-laser excitation, anisotropy measurements thus provide information on energy- and hole-transfer self-exchange dynamics that are central to this report.

We note that fluorescence anisotropy has widely been utilized as a rotational probe in biophysical assays.[14,15] In such assays, θ is calculated in the same manner as described herein and is often referred to as the rotational correlation time. In the present work, θ is now understood to be a self-exchange correlation time, and hence, its significance differs from that of physical rotation of molecules. The surface-anchored molecules are not undergoing rotational diffusion; instead, the loss in anisotropy over time is due to lateral self-exchange reactions that translate the energy or charge around the spherical nanoparticle.

Scheme 1. Cross Section of a Hypothetical Molecule−TiO_2 Arrangement for Ru-Trisbipyridyl Coordination Compounds Anchored to a Spherical TiO_2 Nanocrystallite[a]

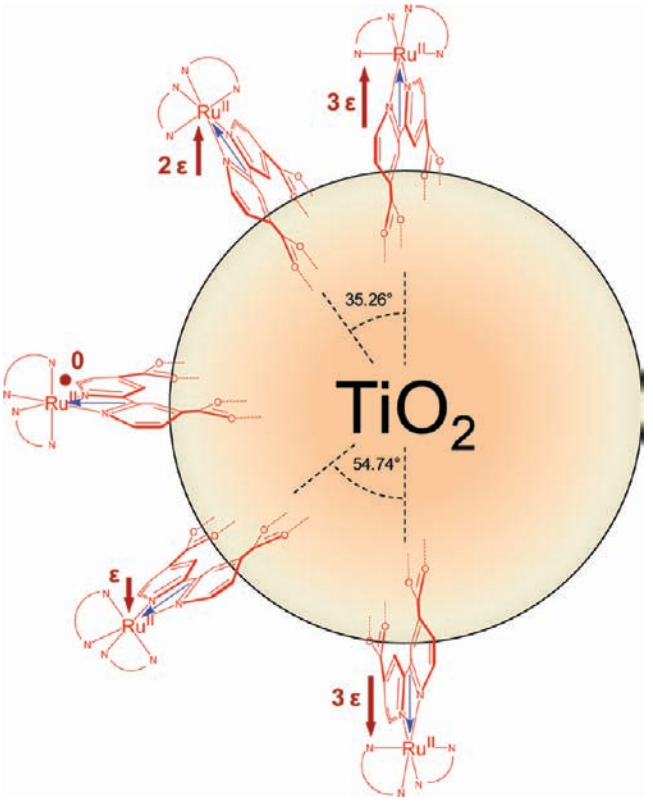

[a] For the sake of clarity, only five molecules are depicted while ~400 are expected for each anatase nanocrystallite (~15 nm in diameter). Polarized light excitation was assumed to be vertical, propagating in the plane of the page, with detection in the direction of the reader.

This anisotropy approach enabled the determination of self-exchange kinetic data under conditions where unwanted recombination processes were operative. Self-exchange energy transfer occurred in competition with excited-state decay, while self-exchange hole transfer often occurred on the time scale of interfacial charge recombination. The results presented below indicate that interfacial self-exchange energy-transfer reactions are many orders-of-magnitude faster than hole-transfer reactions at these sensitized TiO_2 interfaces. Furthermore, hole transfer was found to be sensitive to the identity of the ruthenium−polypyridyl compound and the chemical environment. The implications of these findings for solar energy conversion are discussed.

EXPERIMENTAL SECTION

Materials. The following reagents and substrates were reagent grade or better and were used as received from the indicated commercial suppliers: acetonitrile (Burdick & Jackson, spectrophotometric grade); absolute, anhydrous ethanol (Pharmco−Aaper, ACS/USP grade, > 99.5%); methanol (Sigma−Aldrich, spectrophotometric grade, > 99.9%); acetone (bulk solvent); lithium perchlorate (Aldrich, 99.99%); tetra-*n*-butylammonium perchlorate (TBAClO_4; Fluka, > 99.9%); tetra-*n*-butylammonium

hydroxide (TBAOH; Fluka, 1 M aqueous); cobalt(III) *meso*-5,10,15,20-tetrakis(4-carboxyphenyl)porphyrin chloride (Frontier Scientific); argon gas (Airgas, > 99.998%); oxygen gas (Airgas, industrial grade); titanium(IV) isopropoxide (Sigma–Aldrich, 97%); zirconium(IV) propoxide (Aldrich, 70 wt % solution in 1-propanol); fluorine-doped, SnO_2-coated glass (FTO; Hartford Glass Co., Inc., 2.3 mm thick, 15 Ω/□); and glass microscope slides (Fisher Scientific, 1 mm thick). The sensitizers employed were available from previous studies: $[Ru(dtb)_2(dcb)](PF_6)_2$,[16] where dtb is 4,4′-$(C(CH_3)_3)_2$-2,2′-bipyridine and dcb is 4,4′-$(COOH)_2$-2,2′-bipyridine; $[Ru(bpy)_2(deebq)](PF_6)_2$,[17] where bpy is 2,2′-bipyridine and deebq is 4,4′-diethyl ester-2,2′-biquinoline; Z907,[16] *cis*-$Ru(dnb)(dcb)(NCS)_2$, where dnb is 4,4′-$(CH_3(CH_2)_8)_2$-2,2′-bipyridine; and N3,[18] *cis*-$Ru(dcb)_2(NCS)_2$.

Sensitized Metal Oxide Thin Film. Transparent TiO_2 nanocrystallites (anatase, ∼15 nm in diameter) and ZrO_2 nanoparticles were prepared by hydrolysis of the appropriate precursors [Ti(*i*-OPr)$_4$ or Zr(OPr)$_4$] using a sol–gel technique previously described in the literature.[9] The sols were cast as mesoporous thin films using Scotch transparent film tape as a spacer (∼10 μm thick) by doctor blading onto glass microscope slides for spectroscopic measurements and transparent FTO conductive substrates for electrochemical measurements. In all cases, the thin films were annealed at 420 °C for 30 min under O_2 flow. Imaging of platinum-sputtered thin film samples on FTO substrates was performed with a JEOL JSM-6700F cold cathode field emission scanning electron microscope (SEM) to determine the average nanoparticle size.

Thin films were first pretreated with aqueous base (TBAOH, pH 11) for 15 min followed by an acetone wash and heated to 75 °C. The films were then briefly placed in the neat solvent that was to be used for surface binding to wet the surface with the desired solvent. Sensitization for all coordination compounds was achieved by immersing the supported thin films in sensitizer solutions (nanomolar to millimolar concentrations) for minutes to days. Low surface coverage films were prepared by overnight reactions in low concentration dying solutions. Films were then immersed in the neat solvent that was used for sensitizer binding, acetonitrile, absolute ethanol, or DMSO, for 5–10 min, followed by a thorough washing with the experimental solvent. Unless noted otherwise, the thin films were sensitized to roughly maximum surface coverage $\Gamma \approx (5-7) \times 10^{-8}$ mol/cm^2, which was calculated by a previously published method.[11] Briefly, the molar decadic extinction (absorption) coefficient (ε in M^{-1} cm^{-1}) at the maximum of the metal-to-ligand charge transfer transition was assumed to be the same in solution *and on the surface*. This value was used along with the modified Beer–Lambert law formula to calculate a macroscopic surface coverage (Γ in mol/cm^2) by eq 3,

$$\mathrm{Abs} = \varepsilon c l = 1000 \times \varepsilon \Gamma \tag{3}$$

The samples were then positioned diagonally in a 1 cm cuvette containing the experimental solution. For transient absorption and electrochemical studies, the cuvettes containing the sample and electrolyte solution were purged with Ar(g) for at least 30 min prior to experimentation. Unless noted otherwise, all thin films were sensitized to near maximum surface coverage and immersed in Ar-purged acetonitrile at 21 °C.

Spectroscopy. *UV–Visible Absorption.* Steady-state UV–visible absorbance spectra were obtained on a Varian Cary 50 spectrophotometer at room temperature.

Nanosecond transient absorption measurements were obtained with an apparatus similar to that which has been previously described.[19] Briefly, samples were excited by a Q-switched, pulsed Nd:YAG laser [Quantel USA (BigSky) Brilliant B; 5–6 ns full width at half-maximum (fwhm), 1 Hz, ∼10 mm in diameter] directed 45° to the film surface and tuned to vertically polarized 532 nm light with the appropriate nonlinear optics. An H_2-filled Raman shifter (∼400 psi) was employed to obtain Stokes-shifted 683 nm excitation. A polarizer was employed even though the vertical polarization was nearly maintained due to the extremely small depolarization ratio of H_2.[20−22] The excitation fluence was measured by a thermopile power meter (Molectron) and was ∼200 μJ/pulse so that the absorbed fluence was typically ≤50 μJ/pulse, unless noted otherwise. A 150 W xenon arc lamp served as the probe (Applied Photophysics) and was aligned orthogonal to the laser excitation light. Before arriving at the sample, the probe was directed through a 1/4 m monochromator (Spectral Energy Corp., GM 252). For detection on sub-100 μs time scales, the lamp was pulsed with 100 V. Detection was achieved in a T format with a monochromator (Spex 1702/04) optically coupled to an R928 photomultiplier tube (Hamamatsu). For some measurements a Glan–Taylor polarizer positioned at the magic angle (∼54.7°) relative to the polarization of the excitation light was placed before the detection monochromator to remove polarization-dependent signals. Transient data was acquired on a computer-interfaced digital oscilloscope (LeCroy 9450, Dual 350 MHz). The instrument response time was ∼10 ns. Typically, 100 laser pulses were averaged at each observation wavelength and two to six identical measurements were taken and averaged, to help increase the signal-to-noise ratio of the magic angle and anisotropy data.

All measurements employed an excitation polarizer (P_{ex}) before the sample and a detection polarizer (P_{det}) after the sample. For anisotropy measurements, P_{ex} was set to vertical, the same polarization of the laser, and P_{det} was set to either vertical (V) or horizontal (H) such that the magic angle and anisotropy values could be calculated via eqs 4 and 5,[14,15] respectively

$$\Delta\mathrm{Abs}_{magic\ angle} = \frac{(I_{VV} + 2GI_{VH})}{3} \tag{4}$$

$$\Delta\mathrm{Abs}_{\mathrm{anisotropy}} = \frac{(I_{VV} - GI_{VH})}{3\Delta\mathrm{Abs}_{magic\ angle}} \tag{5}$$

where I_{VY} is the intensity of the detected light with excitation polarization V and detection polarization Y = V or H, and G is a wavelength-dependent correction factor for the polarization-dependent response of the detection system. Corrections for the wavelength-dependent polarization response were not necessary in the transient absorption data due to their cancellation during calculation of ΔAbs, and thus G = 1. Unless specifically mentioned, all time-resolved pump–probe experiments were performed under conditions where less than one excited-state was formed per nanoparticle.

Photoluminescence. Steady-state photoluminescence (PL) measurements were obtained with a fluorimeter (SLM Instruments SLM-48000S) employing a Rhodamine B/ethylene glycol "quantum counter". The PL spectra were collected near room temperature and were corrected for the wavelength-dependent response of the excitation and emission detection systems by calibration with a tungsten–(halogen) irradiance-standard lamp. The SLM Instruments SLM-48000S consisted of a single excitation monochromator (MC200) optically coupled to a 450 W xenon arc lamp and a single detection monochromator (MC200) with a GaAs photomultiplier tube (Hamamatsu, R928P). The excitation beam was directed 45° to the film surface, and the emitted light was monitored at a right angle. The SSPL spectra were collected at 21.0(1) °C with calcite polarizers and a 585 nm long-pass filter.

Time-resolved PL data were acquired on the same apparatus used for the transient-absorption measurements in an L format. Corrections for the polarization-dependent response of the detection system were achieved by calculating G factors. A two-mirror beam-steering device was used to convert the polarization of the excitation laser to a ∼45° linear polarization, so that the correction factor, G, could be measured. This allowed for in situ correction of the wavelength-dependent polarization response of the detection system for each sample by setting

Scheme 2. Chemical Structures of the Transition-Metal Coordination Compound Sensitizers, and Their Abbreviations, Used in the Studies

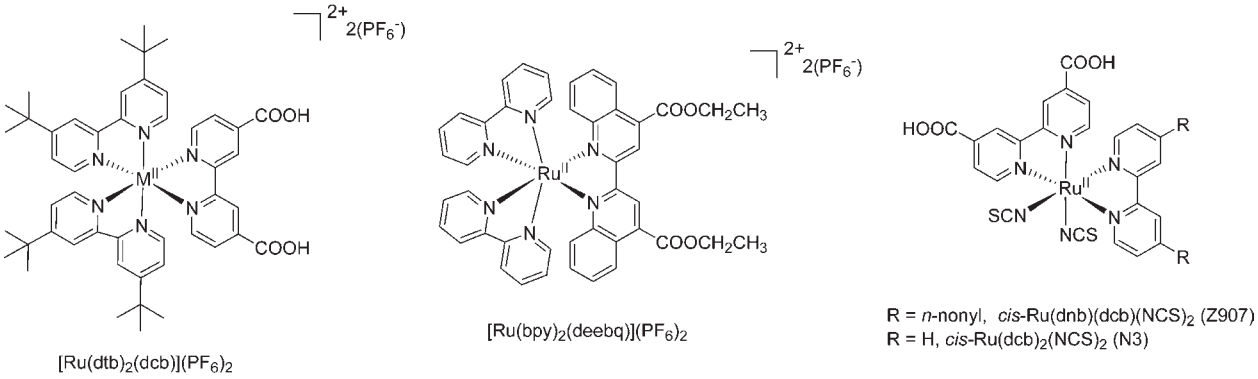

P_{ex} to horizontal so that the correction factor, $G = I_{HV}/I_{HH}$, could be calculated. See the Supporting Information for further details of the correction method. For each wavelength, the calculated G factor was then used to scale the I_{VH} values as explicitly written in eqs 4 and 5.

Variable-temperature PL spectra were acquired with a Neslab ULT95 bath circulator equipped with a four-window Dewar filled with methanol. The temperature was monitored with a thermocouple probe (Omega DPi32) and was allowed to equilibrate at each temperature for at least 15 min prior to a measurement. For measurements at ~77 K, a 2−3 mm wide sample was submerged in MeOH:EtOH (~1:4, v/v) in a standard NMR tube and immersed into an N_2(l)-filled glass coldfinger Dewar such that only about half of the MeOH:EtOH solution was submerged in N_2(l). The resultant solvent glass cracked ~80% of the time, and those that did not crack were used.

Electrochemistry. A potentiostat (Epsilon electrochemical analyzer) was employed for measurements in a standard three-electrode arrangement with a sensitized TiO_2 thin film deposited on an FTO substrate working electrode, a Pt gauze counter electrode, and an aqueous Ag/AgCl (NaCl saturated) reference electrode (Bioanalytical Scientific Instruments, Inc.). The ferrocenium/ferrocene $[Fe(Cp)_2^{+/0}]$ half-wave potential measured in a 200 mM $LiClO_4$ acetonitrile electrolyte was used as an internal standard. Conversion to normal hydrogen electrode (NHE) used the published values for the reference electrode, i.e. +197 mV vs NHE,[23] and corrected for the expected $E_{1/2}(Fe(Cp)_2^{+/0})$ of +310 mV vs the KCl-saturated aqueous calomel electrode (SCE), where SCE is +241.2 mV vs NHE.[23]

Computation. *Data Analysis.* Kinetic and spectral data were modeled in Origin 7.0. Least-squares error minimization was accomplished with the Levenberg−Marquardt iteration method. The photoluminescence kinetic data were smoothed via adjacent averaging (±5 points) before calculating the magic-angle and anisotropy data. The transient-absorption kinetic data were first converted to log-time space and then interpolated to 0.01 logarithmic deviations, followed by smoothing via adjacent averaging (±5 points). For the spectral modeling, a method for the standard addition of known spectra, written in the C programming language, was implemented in Origin's error minimization routine.

Simulations of Anisotropy Data. Monte Carlo simulations to model the energy-transfer anisotropy decay kinetics and calculate the average number of self-exchange hole-transfer reactions required to reach a metalloporphyrin catalyst were performed with Wolfram Mathematica 7.0 on a PC running an Intel Core2 Duo CPU P9700 at 2.79 GHz.

RESULTS

The heteroleptic sensitizers utilized for the self-exchange studies along with their abbreviations are shown in Scheme 2.

Figure 1 depicts normalized magic-angle photoluminescence (PL) excitation and PL spectra for $Ru(dtb)_2(dcb)/ZrO_2$ immersed in neat acetonitrile at room temperature in the presence and absence of $LiClO_4$. The excitation spectra were found to be in good agreement with the absorptance spectra, which is related to the absorbance by $1 - 10^{-Abs}$, measured under the same conditions. Broad overlapping Ru → dcb and Ru → dtb metal-to-ligand charge transfer (MLCT) absorptions bands were observed in the visible region (Figure S1a, Supporting Information). The absorption and PL spectra displayed a noticeable red shift in the presence of this electrolyte; however the PL excitation spectra varied very little (Figure S2a, Supporting Information). The PL intensity decreased in the presence of $LiClO_4$ (data not shown). The absorption spectrum of $Ru(bpy)_2(deebq)/ZrO_2$[17] displayed well-resolved Ru → deebq (550 nm) and Ru → bpy (450 nm) MLCT absorption bands (Figure S1b, Supporting Information). The absorption spectra of all compounds were the same within experimental error when anchored to ZrO_2 or TiO_2 thin films.

At low laser fluences, the magic angle and anisotropy time-resolved PL kinetics were well-modeled as first-order decay processes, eq 6

$$I = I_o \exp\left[-\left(\frac{t}{h}\right)\right] \quad (6)$$

where for PL kinetics I = PL and h is the characteristic lifetime, τ, and for anisotropy kinetics $I = r$ and h is the anisotropy correlation time constant, θ_{ent}. Mean values from multiple measurements/samples were reported with standard deviation of the final digit in parentheses. The kinetics was independent of the monitoring wavelength beyond 625 nm with lifetime [τ = 1.04(3) vs 0.68(1) μs] and anisotropy correlation time [θ_{ent} = 2.8(3) vs 2.0(3) μs] in the absence and presence of $LiClO_4$, respectively. The most significant effect introduced by addition of $LiClO_4$ was a decrease in the excited-state lifetime with lesser change in the PL anisotropy (Figure S2b, Supporting Information).

Monte Carlo simulations under vertically polarized simulated low light conditions, i.e., only one excited state per nanoparticle, could accurately reproduce the first-order anisotropy decays, with the nearest-neighbor hopping time constant as the only adjustable parameter. The energy-transfer model employed spherical nanoparticles (15 nm in diameter) with a maximum, near evenly distributed packing of sensitizers longitudinally and latitudinally at a minimum of van der Waals contact (7 Å)[24] (Scheme 3a). The initial excited-state distribution was randomly

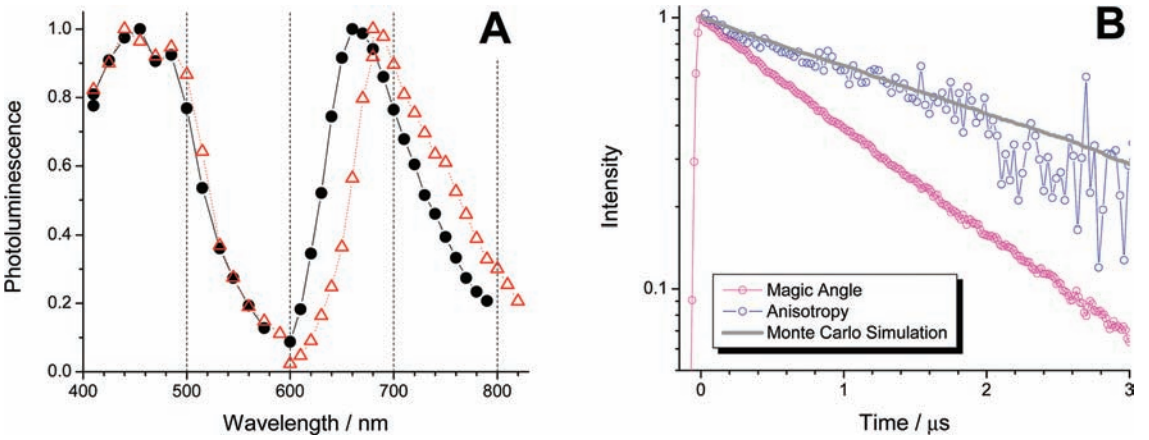

Figure 1. (A) Normalized magic angle photoluminescence (PL) spectra for a $Ru(dtb)_2(dcb)/ZrO_2$ thin film before (filled black circles) and after (open red triangles) introduction of 100 mM $LiClO_4$. Photoluminescence spectra (right) were acquired with λ_{ex} = 532 nm, while excitation spectra (left) were monitored at the PL maxima ($\lambda_{mon\text{-}neat}$ = 650 nm, $\lambda_{mon\text{-}Li+}$ = 680 nm). (B) Normalized magic angle (open magenta circles) and anisotropy (open blue circles) PL changes (λ_{mon} = 700 nm) after pulsed 532 nm laser excitation (λ_{ex} = 532 nm) for the thin film from panel A immersed in neat acetonitrile, on a logarithmic intensity scale. Overlaid on the anisotropy changes, as a solid gray line, is a representative Monte Carlo simulation from which a Dexter energy-transfer hopping rate constant of $(710\ ns)^{-1}$ was abstracted.

selected in spherical polar coordinates with equal circular latitudinal weights and longitudinal weights of $(\cos^2\phi)$ with appropriate $(\sin\phi)$ degeneracy, where ϕ is the inclination angle. Energy transfer at any distance beyond van der Waals contact was modeled by a Dexter-type mechanism with an exponential decay for the probability of transfer, β_{tunnel}. Given β_{tunnel} = 0.35 $Å^{-1}$, which was determined previously for energy-transfer processes between metal−polypyridyl compounds on ZrO_2[25] and by far represents a lower limit for most solvents,[26] a transfer to a non-nearest-neighbor occurred, on average, about once per 60 simulated hops.

The probability that an excited state hopped to any other molecule was calculated using the rate constant at van der Waals contact, the degeneracy of each hop (i.e., the number of locations per circular latitude from the excited sensitizer), and an exponentially decaying distance-dependent term employing the electronic-coupling matrix-element β_{tunnel} factor. Random numbers were generated with an extended cellular automaton pseudorandom number generator. Mathematical movement of the excited state was controlled using Quaternion matrices and conversion of the excited state's location to Cartesian coordinates, which allowed for ease of its movement and regeneration of the distribution of neighboring sensitizers.[27] Conversion back to spherical polar coordinates allowed the inclination angle, and thus the relative angular location of the excited molecule versus the initial vertical polarization of the excitation light, to be retained. This also made calculation of the anisotropy straightforward via eq 7,[28]

$$r = \frac{3\langle\cos^2\phi\rangle - 1}{2} \qquad (7)$$

where $(\cos\phi)$ for each sensitizer was simply the cosine of its inclination angle stored in the spherical polar coordinate matrix. This process was repeated for a given number of iterations (Scheme 3b), corresponding to an amount of time, and then the resulting anisotropy decay was generated. Care was taken such that the probability of a transfer event per time period, i.e. frequency factor, was <1%, so as not to mistakenly miss two hopping events per random number generated. Under conditions of maximum sensitizer coverage, the experimental data was well-modeled using a

Scheme 3. Monte Carlo Simulations for a Maximum Packing Coverage of Ru−Trisbipyridyl Coordination Compounds on a Spherical Nanocrystallite[a,b]

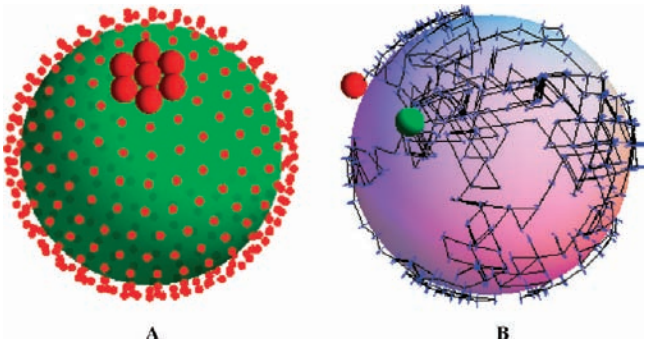

[a] Even distribution of molecules (red spheres) anchored to a 15 nm diameter nanocrystallite, assuming a 7 Å van der Waals radius, which is depicted for the seven molecules at the top pole. [b] Monte Carlo simulation (−) for energy transfer across a single nanocrystallite, based on a Dexter mechanism, for the initial distribution shown in panel A from the initially photoexcited molecule (green sphere) to the final molecule (red sphere) in the simulation. Also shown as blue arrows are the approximate transition dipole moments for the excited states involved in the simulation.

rate constant per energy transfer "hop" of $(120\ ns)^{-1}$, which included nearest-neighbor degeneracy, and thus $(710\ ns)^{-1}$ for a single self-exchange reaction (Figure 1b).

The absorption spectra of one of the highest (5.0×10^{-8} mol/cm^2) and one of the lowest (7×10^{-9} mol/cm^2) $Ru(dtb)_2(dcb)/ZrO_2$ surface-coverage thin films are depicted in Figure 2a. PL decays measured at the magic angle and anisotropy kinetics for the same materials are shown in Figure 2b. At low surface coverage, the excited-state lifetime was within error the same, whereas the rate of anisotropy decay decreased slightly. In general, there was only a minor increase in the anisotropy decay rate with surface coverage (Figure S3, Supporting Information). Note that the initial fundamental anisotropy at 700 nm was significantly smaller than the theoretical maximum of 0.4 for both surface

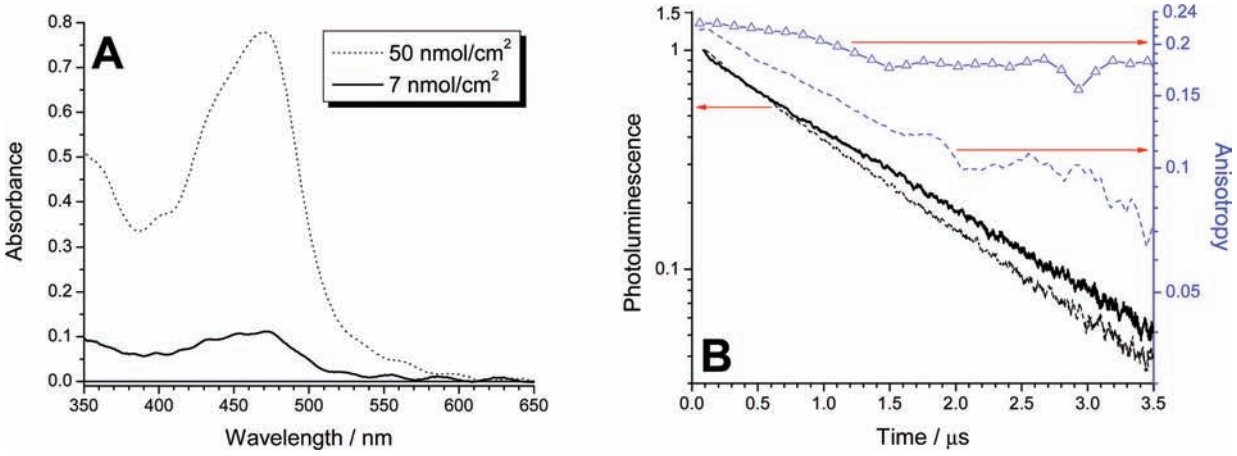

Figure 2. (A) UV−Vis absorption spectra of two $Ru(dtb)_2(dcb)/ZrO_2$ thin films immersed in Ar-purged neat acetonitrile at 21 °C at the indicated surface coverages. (B) PL magic-angle (bottom data; left axis) and anisotropy (top data; right axis) changes (λ_{ex} = 532 nm, λ_{mon} = 700 nm) for the thin films from panel A, where the dashed kinetics correspond to the sample with the higher surface coverage, on logarithmic intensity scales. Similar behavior was also observed for $Ru(dtb)_2(dcb)/TiO_2$ thin films (Figure S3, Supporting Information).

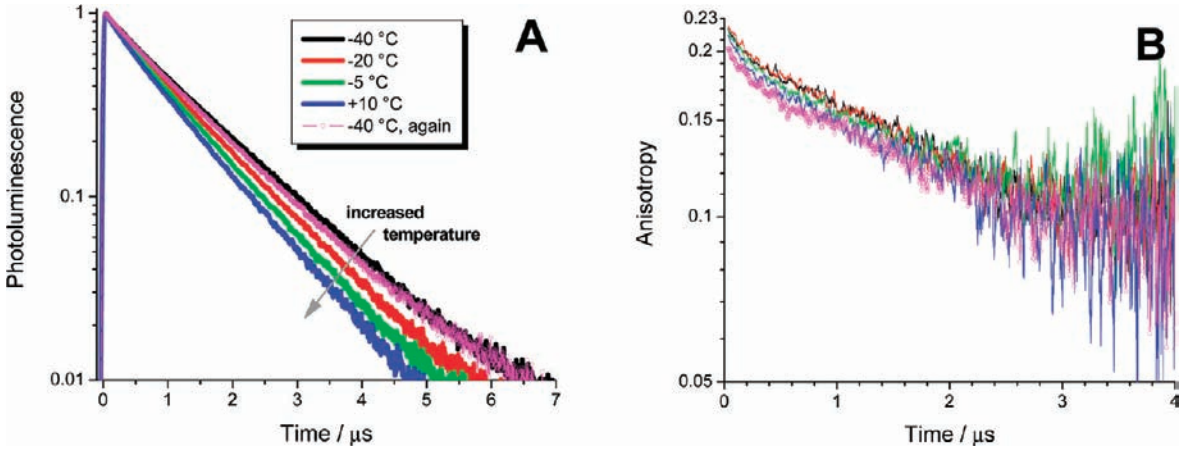

Figure 3. (A) Normalized magic angle and (B) anisotropy PL changes (λ_{ex} = 532 nm, λ_{mon} = 700 nm) of a $Ru(dtb)_2(dcb)/ZrO_2$ thin film immersed in Ar-purged, neat acetonitrile at the indicated temperatures (°C), on logarithmic intensity scales. Similar behavior was also observed for a $Ru(dtb)_2(dcb)/TiO_2$ thin film in a solvent glass (Figure S4, Supporting Information).

coverages, $r_o \approx 0.21(3)$. The initial anisotropy increased to ~0.35 when a $Ru(bpy)_2(deebq)/ZrO_2$-sensitized thin film was used under otherwise identical conditions, which is reflected in its steady-state PL spectrum at long wavelengths (Figure S1b, Supporting Information).

Figure 3 depicts the temperature-dependence of the magic angle and anisotropy PL signals of a $Ru(dtb)_2(dcb)/ZrO_2$ thin film. Both the magic angle and anisotropy PL signals were well-described by a first-order kinetic model when monitored from 650 to 750 nm. Temperature-dependent magic angle kinetics were apparent, τ = 0.97 vs 2.8 μs for 283 and 77 K, respectively; however, the anisotropy signal was nearly temperature-independent (Figure 3b and Figure S4b, Supporting Information). From the magic angle PL kinetics at four temperatures, an activation energy of 230 cm^{-1} and frequency factor of 3.4 × 10^6 s^{-1} were abstracted via an Arrhenius analysis (Figure S4c, Supporting Information).

Figure 4 depicts the fluence dependence to the magic angle and anisotropy PL decays of $[Ru(dtb)_2(dcb)]^{2+}$ anchored to TiO_2 thin films immersed in neat acetonitrile; data using ZrO_2 was the same within error (Figure S5, Supporting Information). The initial fundamental anisotropies were, within error, the same but decayed with an increasing fraction of second-order relaxation as the pulsed 532 nm laser excitation fluence was increased. The decays exhibited long-time limiting anisotropies, $r_\infty \approx 0$, as explained in the Supporting Information.

To promote excited-state injection, a $Ru(dtb)_2(dcb)/TiO_2$ thin film was immersed in a 10 mM $LiClO_4/CH_3CN$ electrolyte. This increased the yield for excited-state injection, but not to unity. The magic angle and anisotropy signals for PL at 700 nm and transient absorption at 486 nm after pulsed 532 nm laser excitation at 2.5 mJ/cm^2 are shown in Figure 5. The entire PL decays were nonexponential and well-described by a parallel first- and second-order kinetic model; a best fit resulted in the lifetime of the first-order component of τ = 1.2 μs. The anisotropy kinetics were well-modeled as a first-order kinetic decay process at 300 ns and beyond, resulting in an energy-transfer correlation time, θ_{ent} = 3.3 μs; this value was larger than that obtained under low-fluence conditions, consistent with Figures 4b and S5b (Supporting Information).

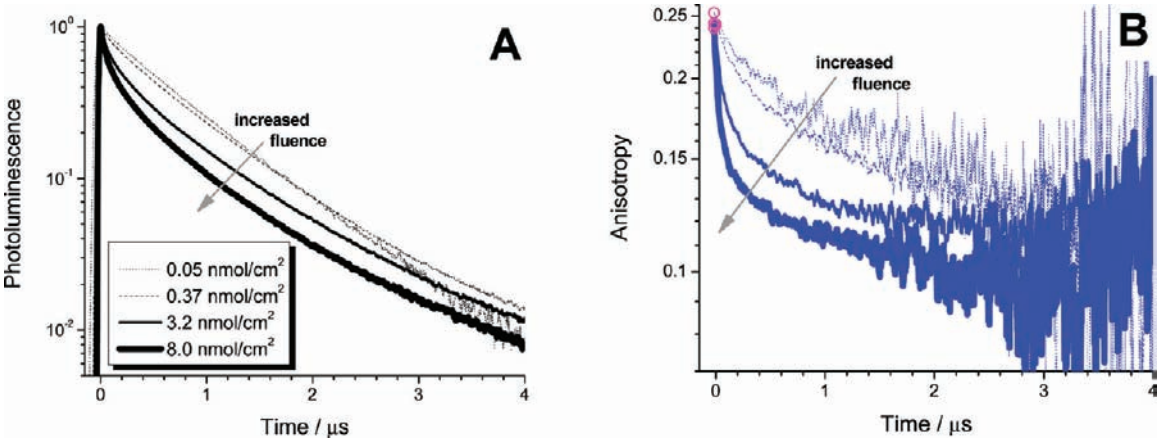

Figure 4. (A) Normalized magic angle and (B) anisotropy PL changes (λ_{ex} = 532 nm, λ_{mon} = 700 nm) for a $Ru(dtb)_2(dcb)/TiO_2$ thin film immersed in Ar-purged, neat acetonitrile at 21 °C at the indicated absorbed photon fluxes (in nmol/cm^2), using the same key and on logarithmic intensity scales. The initial time points in panel B (open magenta circles) highlight the nearly coincident fundamental anisotropies. Similar behavior was also observed for $Ru(dtb)_2(dcb)/ZrO_2$ thin films (Figure S5, Supporting Information).

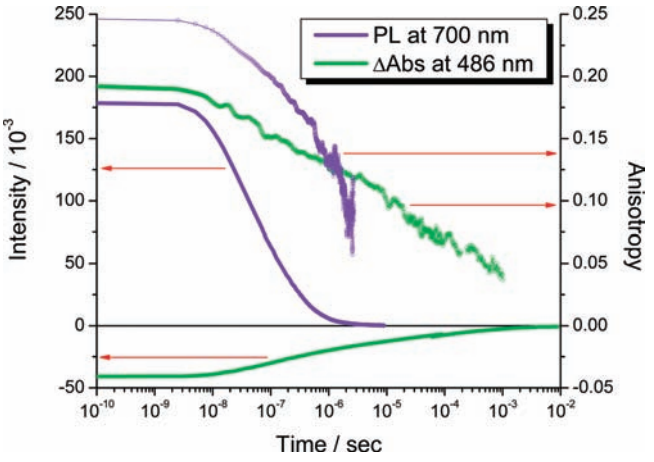

Figure 5. PL (λ_{mon} = 700 nm) and transient-absorption (λ_{mon} = 486 nm), magic angle (bottom data, left axis), and anisotropy (top data, right axis) after pulsed laser excitation (λ_{ex} = 532 nm, 2.5 mJ/cm^2) for a $Ru(dtb)_2(dcb)/TiO_2$ thin film immersed in Ar-purged 10 mM $LiClO_4/CH_3CN$, on a logarithmic time scale.

The measured transient-absorption data were fit to kinetic models on 1 μs and longer time scales to ensure that there were no excited-state contributions, such that $Ru^{III}(dtb)_2(dcb)/TiO_2(e^-) \rightarrow Ru^{II}(dtb)_2(dcb)/TiO_2$ charge recombination was solely observed, where $TiO_2(e^-)$ stands for electrons in TiO_2. The kinetics for charge recombination and the corresponding anisotropy changes were nonexponential but were well-modeled by the Kohlrausch–Williams–Watts (KWW) model as a stretched-exponential function, eq 8

$$I = I_o \exp\left[-\left(\frac{t}{b}\right)^{\beta_{KWW}}\right] \quad (8)$$

where β_{KWW} is inversely related to the width of an underlying Lévy distribution of rate constants, $0 < \beta_{KWW} < 1$, $b = \tau_{KWW}$ or θ_{h+}, $I = \Delta$Abs for transient absorption signals, and the other variables were previously defined. The values obtained for the charge-recombination process were τ_{KWW} = 0.14 μs and β_{KWW} = 0.136, while for the self-exchange hole-transfer process, θ_{h+} = 16.7 μs, using the same β_{KWW} value. Note that a higher laser fluence was required under these low injection conditions to generate enough charge-separated states for anisotropy analysis.

Figure 6a shows the absorption spectra of $Z907/TiO_2$ and $N3/TiO_2$ thin films immersed in neat acetonitrile. Pulsed 683 nm laser excitation of either sensitized thin film resulted in the prompt appearance of a transient-absorption spectrum consistent with an interfacial charge-separated state, comprised of an injected electron in TiO_2 and an oxidized sensitizer, $k_{inj} > 10^8$ s^{-1}. Shown in Figure 6b are magic angle and anisotropy absorption transients monitored at 465 nm. For *cis*-$Ru(dnb)(dcb)(NCS)_2$ it was determined that τ_{KWW} = 14.5 μs and β_{KWW} = 0.183, from the magic angle data, and using the same β_{KWW} value to fit the anisotropy data, the hole-transfer correlation time was determined to be θ_{h+} = 9.6 μs. The anisotropy signals for the *cis*-$Ru(dcb)_2(NCS)_2/TiO_2$ sample displayed little change over the lifetime of the charge-separated state and made quantification of useful kinetic parameters difficult.

Transient absorption anisotropy changes for self-exchange hole transfer were also quantified for $Ru(dtb)_2(dcb)/TiO_2$ (Figure 5). Interestingly, the anisotropy measured after pulsed 532 nm laser excitation of $Ru(dtb)_2(dcb)/TiO_2$ at 465 nm was essentially time-independent when neat acetonitrile was used as the external solvent bath, but a surface-coverage-dependent rate of decay was observed when ≥10 mM $LiClO_4$ was introduced. In contrast, time-resolved anisotropies measured for *cis*-$Ru(dnb)(dcb)(NCS)_2/TiO_2$ were, within experimental error, the same in the presence and absence of 100 mM $LiClO_4$. A comparison of the results for self-exchange energy- and hole-transfer reactions across the surface of sensitized mesoporous thin films is shown in Table 1.

Transient absorption studies of TiO_2 thin films functionalized with CoTCPP [TCPP is *meso*-5,10,15,20-tetrakis(4-carboxyphenyl)porphyrin] and Z907 in a 1:100 molar ratio were also investigated. The strategy was that after excited-state injection into TiO_2, the $Z907^+$ formed was thermodynamically capable of oxidizing the cobalt porphyrin from the formal oxidation state of II to III by lateral hole transfer with a driving force of ΔG° = −1.1 eV. An isotropic distribution of molecules would result in each porphyrin being separated by an average of four Z907

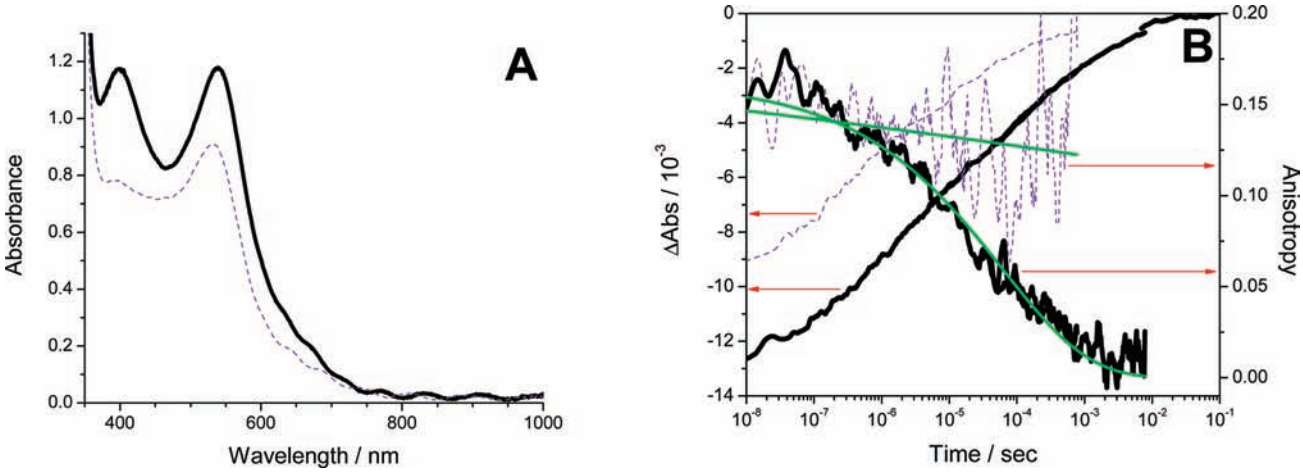

Figure 6. (A) UV−vis absorption spectrum of a *cis*-Ru(dcb)$_2$(NCS)$_2$/TiO$_2$ (black, solid) and a *cis*-Ru(dnb)(dcb)(NCS)$_2$/TiO$_2$ (purple, dashed) thin film immersed in neat acetonitrile. (B) Transient absorption difference magic-angle (left axis) and anisotropy (right axis) changes for the samples in panel A monitored at 465 nm after pulsed laser excitation (λ_{ex} = 683 nm, ~700 μJ/cm^2), using the same color scheme, and on a logarithmic time scale. Overlaid in green, on the anisotropy kinetics, are fits to a stretched exponential function.

Table 1. Photophysical Properties of Ru−Polypyridyl-Sensitized Thin Films in Acetonitrile Solutions at 21 °C Obtained from Time-Resolved Spectroscopic Measurements (λ_{ex} = 532 nm), Monitored at the Indicated Wavelength

sensitizer/film	λ_{mon} / nm	[LiClO$_4$]/mM	$\tau/\mu s$[a]	β_{KWW}	$\theta/\mu s$[b]	r_o	$r_{ss\text{-calculated}}$[c]	Φ[d]
Ru(dtb)$_2$(dcb)*/ZrO$_2$	700	0	1.0	1	2.8	0.20	0.15	0.263
	700	100	0.68	1	2.0	0.22	0.16	0.254
Ru(dtb)$_2$(dcb)*/TiO$_2$	700	10	1.2[e]	1[e]	3.3[e]	0.24	0.18[e]	0.267[e]
Ru^{III}(dtb)$_2$(dcb)/TiO$_2$(e$^-$)	486	10	0.14	0.14	17	0.20	0.20	0.008
Ru^{III}(dnb)(dcb)(NCS)$_2$/TiO$_2$(e$^-$)	465	100	14.5	0.18	9.6	0.17	0.07	0.602

[a] The excited-state lifetime or the interfacial charge-separated-state lifetime. [b] The anisotropy correlation time for energy transfer from first-order excited-state anisotropy decays, θ_{ent}, or the hole-transfer anisotropy correlation time abstracted from analsyis of the charge-recombination kinetics with the KWW function, θ_{h+}. [c] The steady-state anisotropy calculated via the Perrin equation.[28] [d] The calculated quantum yield for randomization of an initial anisotropic population per eq 10. [e] A parallel first- and second-order kinetic model was required to adequately model the data that was acquired at higher laser fluence; solely the first-order components were used to determine r_{SS} and Φ.

sensitizers. Pulsed-light excitation of Z907 resulted in subnanosecond excited-state injection to yield Z907$^+$/TiO$_2$(e$^-$) and the appearance of a very small concentration of oxidized porphyrins, Co^{III}TCPP$^+$. Over hundreds of microseconds, a sharp absorption growth at ~440 nm and bleach at ~420 nm appeared that were expected for oxidation of Co^{II} to Co^{III}. Spectral modeling indicated that by 85 μs, ~10% of the porphyrins had been oxidized with a hole-transfer quantum yield of ~3% based on the number of Z907$^+$ initially created. Control experiments done in the absence of Z907 showed no evidence for oxidation of the porphyrin catalyst.

DISCUSSION

A new photoselection approach to monitor self-exchange reactions between molecules anchored to semiconductor materials enabled the relative rates for isoenergetic, lateral energy- and hole-transfer reactions, and their competing undesirable exergonic recombination reactions, to be quantified. Specifically, it was determined that self-exchange energy-transfer reactions, to randomize initially photoselected anisotropic conditions, occur over the nano- to microsecond time scales. It was also shown that hole-transfer reactions are greatly affected by the choice of sensitizer and electrolyte and occur over longer time scales. The basis for the assignment of the data as being due to self-exchange reactions is described below, followed by a discussion of the relevance of each self-exchange reaction to solar energy conversion.

Assignment as Self-Exchange Reactions. Unlike the situation normally encountered in fluid solution, the anisotropy decay measured for the ruthenium−polypyridyl compounds anchored to TiO$_2$ or ZrO$_2$ mesoporous thin films was not attributed to physical motion of the compounds but to self-exchange energy- or hole-transfer reactions across the surface of the nearly spherical nanoparticles. This assignment was supported by the following observations. Under conditions where the excited-state injection yield was less than unity, the anisotropy decays associated with energy and hole transfer measured on the same sensitized thin film occurred with drastically different rates (Figure 5). If the compounds were indeed mobile, one would anticipate that both the excited and oxidized forms would translate and/or rotate with nearly identical rates, contrary to what was observed. An approximately order-of-magnitude increase in the correlation time between self-exchange energy- and hole-transfer reactions, θ_{ent} = 3.3 μs vs θ_{h+} = 17 μs, respectively, was measured after light excitation of Ru(dtb)$_2$(dcb)/TiO$_2$. Furthermore, if an average hole-transfer correlation time, $\langle\theta_{h+}\rangle$, is calculated as the first moment of the underlying Lévy distribution of rate constants by

the following relation (eq 9),[29]

$$\langle \theta_{h+} \rangle = \left(\frac{\theta_{h+}}{\beta_{\mathrm{KWW}}}\right)\Gamma\left(\frac{1}{\beta_{\mathrm{KWW}}}\right) \quad (9)$$

as suggested by excellent agreement between the experimental data and the Kohlrausch−Williams−Watts kinetic model, another 4 orders of magnitude discrepancy is realized, $\langle \theta_{h+} \rangle$ = 110 ms. Therefore, the extremely disparate rates of anisotropy decay for energy and hole transfer support an underlying mechanism that does not involve physical motion of the compounds.

It was also shown that there was little-to-no measurable temperature dependence to the anisotropy decay associated with energy transfer over a ∼77−283 K range. If the observed anisotropy was indeed physical rotation of the molecules, an inverse temperature dependence to the correlation time would have been expected based on the Stokes−Einstein−Smoluchowski relation. Energy-transfer reactions do not follow Brownian motion and are instead governed by Dexter electron-exchange interaction, Förster dipole−dipole interaction, quantum coherence, trivial emission followed by reabsorption, and/or hybrid or alternative mechanisms. Each has its own temperature dependence to the energy-transfer rate and many display small temperature effects, like that observed here.

Energy-Transfer Reactions. Energy transfer assemblies have been reported previously in dye-sensitized solar cells. An early strategy was to covalently link energy-transfer donors to a central unit that accepted the charge and subsequently transferred an electron to TiO_2.[30−36] If the energy-transfer donors did not increase the molecular footprint of the central unit on the semiconductor surface, the light harvesting efficiency could be enhanced. Indeed, the trinuclear Ru^{II}−compound utilized in the celebrated 1991 *Nature* paper[5] was designed to function as such an antenna.[33] An issue with the *cis*-$Ru(dcb)_2(CN)_2$ acceptor group used was the cis geometry of the ambidentate cyano ligands, which resulted in a footprint that increased with the number of Ru^{II} chromophores. In this regard, a trans geometry was more preferred.[37] A related approach that did not require synthesis of elaborate molecules involved introduction of an energy-transfer donor in the electrolyte that harvested and transferred energy to a surface-anchored compound. This was recently realized by McGehee, Grätzel, and colleagues using an efficient organic energy-transfer donor in the electrolyte surrounding a phthalocyanine-sensitized TiO_2 thin film.[6] Since then, other research groups have investigated the same phenomenon and have realized similar successes.[7,38−41]

Most relevant to the studies described herein, evidence for lateral energy transfer between ruthenium−polypyridyl compounds anchored to the same surface has been reported. Kinetic data at high laser fluences and high surface coverages were found to obey a second-order, equal-concentration mechanism at early times attributed to triplet−triplet annihilation reactions that resulted from lateral self-exchange energy transfer.[42−44] Studies of films cosensitized with Ru(II) and Os(II) chromophores later provided more direct evidence for the lateral energy transfer.[25] Monte Carlo simulations of the fluence-dependent data revealed an energy-transfer, nearest-neighbor hopping rate constant of $(30\ \mathrm{ns})^{-1}$ for $Ru(bpy)_2(dcb)/TiO_2$.[44] This value is in reasonable agreement with $(120\ \mathrm{ns})^{-1}$ abstracted from the maximum surface-coverage anisotropy data herein, where the minor discrepancies could be due to the bulky *tert*-butyl groups, which may slow energy transfer measurably. In addition, the previously reported $(30\ \mathrm{ns})^{-1}$ hopping rate constant was obtained when hops to beyond nearest neighbors were forbidden; when modeled with this assumption, the hopping rate constant from this work was $(110\ \mathrm{ns})^{-1}$.

What follows is a discussion of the anisotropy's dependence on the sensitizer employed, its surface coverage, the solution temperature, and the excitation laser fluence. Interestingly, an initial fundamental anisotropy, $r_o > 0.3$, was not attained for $[Ru(dtb)_2(dcb)]^{2+*}$ anchored to TiO_2 or ZrO_2. As the thermally equilibrated excited (thexi) state is proposed to be well-formulated as $[Ru(dtb)_2(dcb^-)]^{2+*}$, excitation into the Ru → dcb transition should yield the theoretical maximum anisotropy value for randomly distributed chromophores, i.e., r_o = 0.4, while excitation into either of the doubly degenerate opposing dtb ligands should yield a negative initial fundamental PL anisotropy.[45,46] Notwithstanding, anisotropies less than the theoretical maximum of 0.4 are typical for Ru(II)−polypyridyl compounds, where multiple and overlapping charge-transfer transitions are present.[45−47] To test this notion, the steady-state PL excitation anisotropy spectrum for a sample containing $[Ru(bpy)_2(deebq)]^*/ZrO_2$ was investigated. This compound was chosen as it has a single well-resolved Ru → deebq absorption band in the red portion of the visible spectrum, which is significantly separated from the blue Ru → bpy transitions, and a short excited-state lifetime, i.e., $\tau \approx 245$ ns, which attenuates significant energy transfer, and thus anisotropy loss, during excited-state decay. Steady-state PL anisotropy values as high as 0.35 and as low as −0.03 resulted, which agreed reasonably well with the fundamental anisotropies obtained from time-resolved PL measurements. Therefore, the low initial fundamental anisotropies likely resulted from overlapping charge-transfer electronic transitions. Thin films of ZrO_2, instead of TiO_2, were chosen initially so as to exclude side effects due to other phenomena that often occur under conditions of favorable excited-state electron injection into TiO_2.[18,48−50]

The surface-coverage dependence for energy transfer was small. As the energy-transfer mechanism involves interactions between a singlet ground state and a predominantly triplet excited state,[51−54] a Dexter energy-transfer mechanism previously has been proposed for MLCT excited states. This implies an exponential dependence of the energy-transfer, nearest-neighbor hopping rate constant. Because the experimentally observable parameters were the self-exchange correlation times and the sensitizer surface coverage or number of sensitizers per nanoparticle, deduced from absorption measurements, Monte Carlo simulations were performed to determine how these parameters were related. It was confirmed that, under the conditions given in the Experimental Section, the nearest-neighbor distance was proportional to the square root of the inverse of the number of sensitizers per particle (Figure S6a, Supporting Information). It was also determined that the logarithm of the nearest-neighbor energy transfer rate constants and logarithm of the self-exchange correlation times were linearly related to one another (Figure S6b, Supporting Information). The experimental data did not show a clear exponential dependence for energy transfer, which implied that intermolecular energy transfer may not be the only mechanism resulting in a loss of anisotropy (Figure S3, Supporting Information).

A small temperature dependence to the energy-transfer self-exchange was measured at low laser fluences. The quantum yield for randomization, Φ, of an initial anisotropic population was

calculated per the following equation

$$\Phi = \frac{\tau}{\tau + \theta_{ent}} \quad (10)$$

where τ is the excited-state lifetime and θ_{ent} is the energy-transfer correlation time.[28] The Φ parameters are given in Table 1 and assist in quantifying the effectiveness by which a molecule can deliver its free energy to sparsely located "reaction centers". In addition, the temperature required to achieve a certain efficiency can be calculated. For example, for the lifetime measured at 283 K, a $\Phi < 0.20$ quantum yield was obtained. As θ_{ent} was nearly temperature independent over a 200 K range while τ was not, extrapolation of the Arrhenius relation predicted that at ~130 K the excited-state lifetime and energy-transfer correlation time should be equal, $\tau = \theta_{ent}$. Thus, $\Phi = 0.5$, implying that half of the sensitizers in the initially photoselected subpopulation, excited by low fluence excitation, would circumnavigate the nanosphere before relaxing back to the ground state.

The initial anisotropy decay rate increased with laser fluence. A likely explanation for this observation is based on the increased yield of triplet−triplet annihilation reactions previously reported under such conditions.[44] Since the excitation laser light was vertically polarized, the majority of the excited states were generated at the north and south poles along the vertical axes of the nanocrystallites. The close proximity of these excited states suggests that at early times they were removed most rapidly, via annihilation reactions. The excited states that were located near the equator of the nanoparticles were much less likely to have been excited. As such, the resulting low local concentration of chromophores meant little-to-no rapid annihilation reactions near the equator. Since radiative and nonradiative decay are much slower processes, these excited states would decay little over this initial time period. The disparate rates for excited-state deactivation near the poles vs the equator of the nanoparticles were therefore expected to result in a large and rapid initial drop in anisotropy, consistent with the experimental data.

Hole-Transfer Reactions. The change in anisotropy measured after excited-state injection was reasonably attributed to lateral self-exchange hole transfer across the nanocrystalline TiO_2 surface. It is well-known that Ru-polypyridyl sensitizers anchored to these thin films can be fully oxidized in a standard electrochemical cell provided that the surface coverage exceeds a percolation threshold of about 50% of the saturation value.[9−11,13] Potential-step experiments have allowed effective diffusion coefficients for self-exchange hole transfer to be quantified on the minutes time scale. It was of specific interest to see whether this available electrochemical data was correlated in any way to that from these anisotropy measurements. Since the entire mesoporous film was oxidized in the electrochemical studies, the data were expected to be influenced by interparticle hole transfer across necking regions between anatase nanocrystallites. Significant hole transfer between molecules on different TiO_2 nanocrystallites was less likely on the short time scale probed spectroscopically, so the combined techniques represent a powerful approach for characterization of lateral charge transfer on semiconductor materials.

One advantage of anisotropy over electrochemical measurements is that self-exchange hole transfer can be quantified in many environments without the need for high ionic strength electrolytes. Furthermore, hole hopping can be quantified on short time scales and is limited only by excited-state injection, a process that is known to occur on ultrafast time scales under many conditions.[55] The interfacial charge-separated states often last milliseconds, thereby providing a large temporal range for characterization of hole-hopping reactions.[12] The three sensitizers *cis*-$Ru(dcb)_2(NCS)_2$ (N3), *cis*-$Ru(dnb)(dcb)(NCS)_2$ (Z907), and $Ru(dtb)_2(dcb)^{2+}$ were compared for their ability to perform self-exchange hole-transfer reactions in acetonitrile in the absence and presence of 100 mM $LiClO_4$. Under most conditions, hole transfer was observed on a micro- to millisecond time scale. Interestingly, little-to-no hole transfer was evident for $N3^+/TiO_2(e^-)$ over the course of its charge-separated-state lifetime. On the other hand, another bis-isothiocyanate-based sensitizer, $Z907^+/TiO_2(e^-)$, was found to hole transfer regardless of the presence of a supporting electrolyte. The significant transient-absorption anisotropy kinetics indicative of lateral self-exchange hole transfer observed for $Z907^+/TiO_2(e^-)$ but not $N3^+/TiO_2(e^-)$ is consistent with previous electrochemical measurements made on much longer time scales and was attributed to the molecular−surface orientation.[13] For $N3/TiO_2$, two carboxylic acid groups on opposite dcb ligands, which are trans to the isothiocyanato ligands, were proposed to anchor to TiO_2, whereas for $Z907/TiO_2$ both carboxylate groups of the single dcb ligand bind to TiO_2.[13] As partial hole transfer from Ru^{III} to the isothiocyanto ligands is known, the more radial orientation of the NCS^- ligands relative to the surface in the former compound attenuates rapid intermolecular hole transfer.[12]

Although hole transfer was not observed for $Ru^{III}(dtb)_2(dcb)/TiO_2(e^-)$ in neat acetonitrile, it did occur after introduction of just 10 mM $LiClO_4$. The lack of significant hole-transfer reactions for $Ru^{III}(dtb)_2(dcb)/TiO_2(e^-)$ in neat acetonitrile suggests that ions were required to decrease the work terms associated with self-exchange hole transfer[1] in this more highly charged tris-diimine compound. Heteroleptic ruthenium compounds, like $[Ru^{II}(dtb)_2(dcb)]^{2+}$, anchored to TiO_2 are known to have effective $Ru^{III/II}$ diffusion coefficients of $\sim 3 \times 10^{-10}$ cm^2/s,[13] roughly an order-of-magnitude smaller than that of $Z907^+/TiO_2(e^-)$, due to electron tunneling through the bipyridine ligands.[1] A difficulty in performing a more thorough comparison of the self-exchange hole-transfer rates for these sensitizers is that the functions required to fit their anisotropy kinetics yielded very different distributions of self-exchange hole-transfer rate constants. However, the fact that the distributions and the average hole-transfer correlations times were larger for $Z907^+/TiO_2(e^-)$ indicates that the rates for hole transfer were on average faster for these compounds.

A discrete quantum yield for randomization of the initial anisotropy by hole transfer self-exchange was quantified with eq 10, as was done for energy transfer, where τ was the charge-separated-state lifetime with hole-transfer correlation time, θ_{h+}. The KWW function used to model the data is based on a Lévy distribution of rate constants, where β is inversely related to the width of the distribution of rate constants. Since the β values abstracted from transient data that corresponded to charge recombination and hole hopping were, within experimental error, the same for a given compound, a comparison of any single value within the distribution was of interest. For the data in Table 1, the efficiency of hole hopping for $Ru^{III}(dtb)_2(dcb)/TiO_2(e\text{-})$ was only 0.008 but increased to 0.6 for $Z907^+/TiO_2(e^-)$. Hole transfer self-exchange, while much slower than energy transfer self-exchange, was relatively efficient, as it competed kinetically with the much slower charge recombination process. This data shows that lateral hole transfer can dramatically randomize the initial anisotropy with efficiencies that are markedly dependent on the ruthenium−polypyridyl compound and the environmental conditions.

Scheme 4. Proposed Mechanisms for Multiple-Charge-Transfer Oxidation at a Dye-Sensitized TiO_2 Interface: (A) (1) Lateral Energy Transfer, (2) Excited-State Injection at a Charge-Separation Unit (red box), and (3) Catalysis (Cat) or (B) (1) Excited-State Injection, (2) Lateral Hole Transfer, and (3) Catalysis

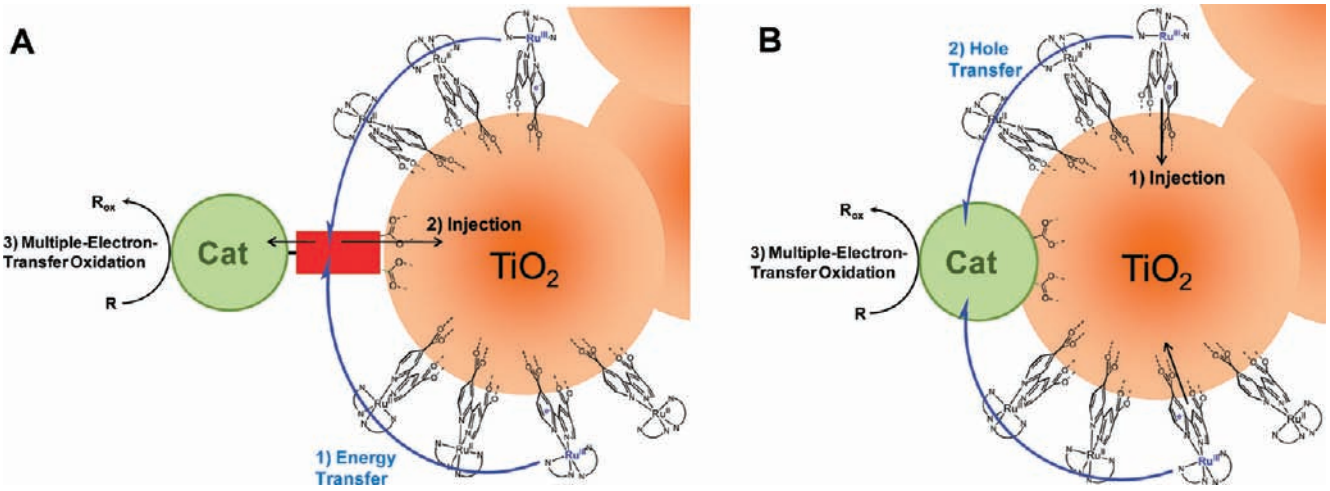

Efficient lateral hole-transfer self-exchange reactions after excited-state injection could be exploited for delivery of multiple redox equivalents to a catalysts capable of water oxidation.[56] In a small step toward this goal, and to test whether lateral hole transfer to *any* catalyst would occur prior to charge recombination, a molecular cobalt compound, CoTCPP, was coanchored to a Z907/TiO_2-sensitized thin film in a 1:100 ratio. The strategy was that after excited-state injection into TiO_2, the oxidized ruthenium−polypyridyl compounds would undergo lateral hole transfer to the catalyst. This was indeed observed to occur on a hundreds of microseconds time scale with a yield of 0.03. The slow time scale for the reaction and low surface coverage of the metalloporphyrin support the hypothesis that Co^{II}TCPP/TiO_2 oxidation was preceded by lateral $Ru^{III/II}$ self-exchange hole transfer. The poor Co^{II} oxidation yields can be rationalized by the large number of hops, kinetic competition with charge recombination, and/or nonuniform loading of CoTCPP. Nevertheless, the experiments were successful and supported our previous results that catalyst oxidation preceded by lateral $Ru^{III/II}$ self-exchange hole transfer did occur (Scheme 4b).[57] To the best of our knowledge, this represents the first direct observation of lateral hole transfer across a semiconductor surface to oxidize a molecular catalyst.[57,58]

While this report focused on characterization of fundamental energy- and hole-transfer self-exchange reactions, it should imminently be possible to utilize them for the photocatalytic oxidation of water (Scheme 4). Energy transfer to a catalyst capable of electron injection into TiO_2 would leave an oxidizing equivalent (hole) on the catalyst. Alternatively, excited-state injection followed by hole transfer could be utilized to deliver an oxidizing equivalent to a catalyst. Accumulation of four holes at a single catalyst is a prerequisite for direct water splitting. In principle, the multiple energy- and charge-transfer reactions required for water splitting could occur after only a few photons were absorbed by chromophores on a single nanoparticle. Photoelectrosynthetic cells that operate by lateral hole transfer to catalysts that accumulate charge and mediate O−O bond formation have indeed been reported.[59] The discovery of a wide variety of water oxidation catalysts based on Ru,[60−64] Ir,[56,59,65−70] Co,[71−75] Mn,[76−80] and Ni[81] indicate that the artificial assembly proposed in Scheme 4 could soon be realized.

CONCLUSIONS

Photoinduced lateral energy- and hole-transfer self-exchange across semiconductor surfaces was observed for the first time by time-resolved spectroscopic anisotropy measurements. The data has clear implications for fundamental studies and for applications in solar energy conversion. First, at a minimum, both photoluminescence and transient-absorption studies of dye-sensitized films that utilize polarized laser sources need employ a depolarizer, without which nonuniform illumination will result. Second, mechanistic models of interfacial charge recombination between $TiO_2(e^-)$s and oxidized sensitizers must take into account diffusion of the injected electron[82] *and* the oxidized sensitizer,[13] not simply the injected electron.[83,84] Third, in the absence of excited-state injection, the mesoscopic TiO_2 thin films developed for regenerative solar cells can function as active "antennae", harvesting sunlight and transferring energy across the surface of nanocrystalline materials. Fourth, lateral hole transfer can be utilized to translate holes present as oxidized sensitizers[85] to catalysts. Such hole transfer is not necessary for iodide oxidation in dye-sensitized solar cells;[55] however, it is required for water oxidation, where four oxidizing equivalents must be accumulated on a single catalytic site.[56] The phenomena presented herein represent two means of concentrating potential energy derived from visible light. If one were able to funnel such energy to molecular catalysts, multiple-charge-transfer reactions that generate solar fuels could be realized. Finally, we anticipate that time-resolved photoluminescence and transient-absorption anisotropy will be useful tools for the study of a wide variety of lateral self-exchange reactions across many classes of semiconductor materials.

ASSOCIATED CONTENT

Supporting Information. Anisotropy data, Arrhenius analysis, and Monte Carlo simulations, and the rationale for the method chosen to correct for the polarization-dependent response of the

detection system are given. This material is available free of charge via the Internet at http://pubs.acs.org.

AUTHOR INFORMATION

Corresponding Author
meyer@jhu.edu

ACKNOWLEDGMENT

We acknowledge support by a grant from the Division of Chemical Sciences, Office of Basic Energy Sciences, Office of Energy Research, U.S. Department of Energy (DE-FG02-96ER14662). S.A. acknowledges a Johns Hopkins University Greer graduate student fellowship. We thank Prof. Ludwig Brand and Dr. Dmitri Toptygin for stimulating discussions on polarization spectroscopy and assistance using their steady-state emission detection system.

REFERENCES

(1) Sutin, N. *Acc. Chem. Res.* **1982**, *15*, 275–282.
(2) Sutin, N. *Prog. Inorg. Chem.* **1983**, *30*, 441–498.
(3) Fleming, G. R.; Scholes, G. D. *Nature* **2004**, *431*, 256–257.
(4) Beljonne, D.; Curutchet, C.; Scholes, G. D.; Silbey, R. J. *J. Phys. Chem. B* **2009**, *113*, 6583–6599.
(5) O'Regan, B.; Grätzel, M. *Nature* **1991**, *353*, 737–740.
(6) Hardin, B. E.; Hoke, E. T.; Armstrong, P. B.; Yum, J.-H.; Comte, P.; Torres, T.; Frechet, J. M. J.; Nazeeruddin, M. K.; Grätzel, M.; McGehee, M. D. *Nat. Photon* **2009**, *3*, 406–411.
(7) Hardin, B. E.; Yum, J.-H.; Hoke, E. T.; Jun, Y. C.; Pechy, P.; Torres, T.; Brongersma, M. L.; Nazeeruddin, M. K.; Grätzel, M.; McGehee, M. D. *Nano Lett.* **2010**, *10*, 3077–3083.
(8) Yum, J.-H.; Baranoff, E.; Hardin, B. E.; Hoke, E. T.; McGehee, M. D.; Nuesch, F.; Grätzel, M.; Nazeeruddin, M. K. *Energy Environ. Sci.* **2010**, *3*, 434–437.
(9) Heimer, T. A.; D'Arcangelis, S. T.; Farzad, F.; Stipkala, J. M.; Meyer, G. J. *Inorg. Chem.* **1996**, *35*, 5319–5324.
(10) Bonhote, P.; Gogniat, E.; Tingry, S.; Barbe, C.; Vlachopoulos, N.; Lenzmann, F.; Comte, P.; Grätzel, M. *J. Phys. Chem. B* **1998**, *102*, 1498–1507.
(11) Trammell, S. A.; Meyer, T. J. *J. Phys. Chem. B* **1999**, *103*, 104–107.
(12) Wang, Q.; Zakeeruddin, S. M.; Cremer, J.; Bauerle, P.; Humphry-Baker, R.; Grätzel, M. *J. Am. Chem. Soc.* **2005**, *127*, 5706–5713.
(13) Wang, Q.; Zakeeruddin, S. M.; Nakeeruddin, M. K.; Humphry-Baker, R.; Grätzel, M. *J. Am. Chem. Soc.* **2006**, *128*, 4446–4452.
(14) Kliger, D. S.; Lewis, J. W.; Randall, C. E. *Polarized Light in Optics and Spectroscopy*; Academic Press, Inc.: Boston, 1990.
(15) Michl, J.; Thulstrup, E. W. *Spectroscopy with Polarized Light*; VCH Publishers, Inc.: Weinheim, Germany, 1986.
(16) Staniszewski, A.; Ardo, S.; Sun, Y.; Castellano, F. N.; Meyer, G. J. *J. Am. Chem. Soc.* **2008**, *130*, 11586–11587.
(17) Hoertz, P. G.; Thompson, D. W.; Friedman, L. A.; Meyer, G. J. *J. Am. Chem. Soc.* **2002**, *124*, 9690–9691.
(18) Ardo, S.; Sun, Y.; Staniszewski, A.; Castellano, F. N.; Meyer, G. J. *J. Am. Chem. Soc.* **2010**, *132*, 6696–6709.
(19) Argazzi, R.; Bignozzi, C. A.; Heimer, T. A.; Castellano, F. N.; Meyer, G. J. *Inorg. Chem.* **1994**, *33*, 5741–5749.
(20) Holzer, W.; Le Duff, Y.; Altmann, K. *J. Chem. Phys.* **1973**, *58*, 642–643.
(21) Le Duff, Y. *J. Phys. B: At. Mol. Phys.* **1981**, *14*, 55.
(22) Bischel, W. K.; Bamford, D. J.; Jusinski, L. E. *Appl. Opt.* **1986**, *25*, 1215–1221.
(23) Bard, A. J.; Faulkner, L. R. *Electrochemical Methods: Fundamentals and Applications*, 2nd ed.; John Wiley & Sons, Inc.: New York, 2001.
(24) Meyer, T. J.; Meyer, G. J.; Pfennig, B. W.; Schoonover, J. R.; Timpson, C. J.; Wall, J. F.; Kobusch, C.; Chen, X.; Peek, B. M.; Wall, C. G.; Ou, W.; Erickson, B. W.; Bignozzi, C. A. *Inorg. Chem.* **1994**, *33*, 3952–3964.
(25) Trammell, S. A.; Yang, J.; Sykora, M.; Fleming, C. N.; Odobel, F.; Meyer, T. J. *J. Phys. Chem. B* **2001**, *105*, 8895–8904.
(26) Gray, H. B.; Winkler, J. R. *Proc. Natl. Acad. Sci. U. S. A.* **2005**, *102*, 3534–3539.
(27) Ericson, T.; Zinoviev, V. *Codes on Euclidean Spheres*; Elsevier: Asterdam, 2001; Vol. 63.
(28) Lakowicz, J. R. *Principles of Fluorescence Spectroscopy*, 3 ed.; Springer Science+Business Media: New York, 2006.
(29) Lindsey, C. P.; Patterson, G. D. *J. Chem. Phys.* **1980**, *73*, 3348–3357.
(30) Balzani, V.; Moggi, L.; Scandola, F. In *Supramolecular Photochemistry*; Balzani, V., Ed.; D. Reidel Publishing Co.: Dordrecht, Holland, 1987; p 1−28.
(31) Bignozzi, C. A.; Argazzi, R.; Indelli, M. T.; Scandola, F. *Sol. Energy Mater.* **1994**, *32*, 229–244.
(32) Bignozzi, C. A.; Argazzi, R.; Scandola, F.; Schoonover, J. R.; Meyer, G. J. *Sol. Energy Mater.* **1995**, *38*, 187–198.
(33) Amadelli, R.; Argazzi, R.; Bignozzi, C. A.; Scandola, F. *J. Am. Chem. Soc.* **1990**, *112*, 7099–7103.
(34) Nazeeruddin, M. K.; Liska, P.; Moser, J.; Vlachopoulos, N.; Grätzel, M. *Helv. Chim. Acta* **1990**, *73*, 1788–1803.
(35) Holten, D.; Bocian, D. F.; Lindsey, J. S. *Acc. Chem. Res.* **2002**, *35*, 57–69.
(36) Forster, R. J.; Keyes, T. E.; Vos, J. G. *Interfacial Supramolecular Assemblies*; John Wiley & Sons Ltd.: Chichester, 2003.
(37) Gajardo, F.; Leiva, A. M.; Loeb, B.; Delgadillo, A.; Stromberg, J. R.; Meyer, G. J. *Inorg. Chim. Acta* **2008**, *361*, 613–619.
(38) Shankar, K.; Feng, X.; Grimes, C. A. *ACS Nano* **2009**, *3*, 788–794.
(39) Basham, J. I.; Mor, G. K.; Grimes, C. A. *ACS Nano* **2010**, *4*, 1253–1258.
(40) Buhbut, S.; Itzhakov, S.; Tauber, E.; Shalom, M.; Hod, I.; Geiger, T.; Garini, Y.; Oron, D.; Zaban, A. *ACS Nano* **2010**, *4*, 1293–1298.
(41) Mor, G. K.; Basham, J.; Paulose, M.; Kim, S.; Varghese, O. K.; Vaish, A.; Yoriya, S.; Grimes, C. A. *Nano Lett.* **2010**, *10*, 2387–2394.
(42) Kelly, C. A.; Farzad, F.; Thompson, D. W.; Meyer, G. J. *Langmuir* **1999**, *15*, 731–737.
(43) Kelly, C. A.; Meyer, G. J. *Coord. Chem. Rev.* **2001**, *211*, 295–315.
(44) Higgins, G. T.; Bergeron, B. V.; Hasselmann, G. M.; Farzad, F.; Meyer, G. J. *J. Phys. Chem. B* **2006**, *110*, 2598–2605.
(45) Wallin, S.; Davidsson, J.; Modin, J.; Hammarström, L. *J. Phys. Chem. A* **2005**, *109*, 4697–4704.
(46) Wallin, S.; Davidsson, J.; Modin, J.; Hammarström, L. *J. Phys. Chem. A* **2005**, *109*, 9378–9378.
(47) Terpetschnig, E.; Szmacinski, H.; Malak, H.; Lakowicz, J. R. *Biophys. J.* **1995**, *68*, 342–350.
(48) Kelly, C. A.; Farzad, F.; Thompson, D. W.; Stipkala, J. M.; Meyer, G. J. *Langmuir* **1999**, *15*, 7047–7054.
(49) Ardo, S.; Sun, Y.; Castellano, F. N.; Meyer, G. J. *J. Phys. Chem. B* **2010**, *114*, 14596–14604.
(50) Cappel, U. B.; Feldt, S. M.; Schoneboom, J.; Hagfeldt, A.; Boschloo, G. *J. Am. Chem. Soc.* **2010**, *132*, 9096–9101.
(51) Crosby, G. A.; Hipps, K. W.; Elfring, W. H. *J. Am. Chem. Soc.* **1974**, *96*, 629–630.
(52) Kober, E. M.; Meyer, T. J. *Inorg. Chem.* **1982**, *21*, 3967–3977.
(53) Meyer, T. J. *Pure Appl. Chem.* **1986**, *58*, 1193–1206.
(54) Juris, A.; Balzani, V.; Barigelletti, F.; Campagna, S.; Belser, P.; von Zelewsky, A. *Coord. Chem. Rev.* **1988**, *84*, 85–277.
(55) Ardo, S.; Meyer, G. J. *Chem. Soc. Rev.* **2009**, *38*, 115–164.
(56) Youngblood, W. J.; Lee, S.-H. A.; Kobayashi, Y.; Hernandez-Pagan, E. A.; Hoertz, P. G.; Moore, T. A.; Moore, A. L.; Gust, D.; Mallouk, T. E. *J. Am. Chem. Soc.* **2009**, *131*, 926–927.
(57) Ardo, S.; Meyer, G. J. *J. Am. Chem. Soc.* **2010**, *132*, 9283–9285.
(58) Kellett, R. M.; Spiro, T. G. *Inorg. Chem.* **1985**, *24*, 2378–2382.
(59) Youngblood, W. J.; Lee, S.-H. A.; Maeda, K.; Mallouk, T. E. *Acc. Chem. Res.* **2009**, *42*, 1966–1973.

(60) Geletii, Y. V.; Botar, B.; Kögerler, P.; Hillesheim, D. A.; Musaev, D. G.; Hill, C. L. *Angew. Chem., Int. Ed.* **2008**, *47*, 3896–3899.
(61) Concepcion, J. J.; Jurss, J. W.; Brennaman, M. K.; Hoertz, P. G.; Patrocinio, A. O. T.; Murakami Iha, N. Y.; Templeton, J. L.; Meyer, T. J. *Acc. Chem. Res.* **2009**, *42*, 1954–1965.
(62) Romain, S.; Bozoglian, F.; Sala, X.; Llobet, A. *J. Am. Chem. Soc.* **2009**, *131*, 2768–2769.
(63) Romain, S.; Vigara, L.; Llobet, A. *Acc. Chem. Res.* **2009**, *42*, 1944–1953.
(64) Xu, Y.; Fischer, A.; Duan, L.; Tong, L.; Gabrielsson, E.; Åkermark, B.; Sun, L. *Angew. Chem., Int. Ed.* **2010**, *49*, 8934–8937.
(65) McDaniel, N. D.; Coughlin, F. J.; Tinker, L. L.; Bernhard, S. *J. Am. Chem. Soc.* **2008**, *130*, 210–217.
(66) Hull, J. F.; Balcells, D.; Blakemore, J. D.; Incarvito, C. D.; Eisenstein, O.; Brudvig, G. W.; Crabtree, R. H. *J. Am. Chem. Soc.* **2009**, *131*, 8730–8731.
(67) Nakagawa, T.; Beasley, C. A.; Murray, R. W. *J. Phys. Chem. C* **2009**, *113*, 12958–12961.
(68) Nakagawa, T.; Bjorge, N. S.; Murray, R. W. *J. Am. Chem. Soc.* **2009**, *131*, 15578–15579.
(69) Blakemore, J. D.; Schley, N. D.; Balcells, D.; Hull, J. F.; Olack, G. W.; Incarvito, C. D.; Eisenstein, O.; Brudvig, G. W.; Crabtree, R. H. *J. Am. Chem. Soc.* **2010**, *132*, 16017–16029.
(70) Tilley, S. D.; Maurin, C.; Sivula, K.; Grätzel, M. *Angew. Chem., Int. Ed.* **2010**, *49*, 6405–6408.
(71) Kanan, M. W.; Nocera, D. G. *Science* **2008**, *321*, 1072–1075.
(72) Jiao, F.; Frei, H. *Angew. Chem., Int. Ed.* **2009**, *48*, 1841–1844.
(73) Kanan, M. W.; Surendranath, Y.; Nocera, D. G. *Chem. Soc. Rev.* **2009**, *38*, 109–114.
(74) Nocera, D. G. *Inorg. Chem.* **2009**, *48*, 10001–10017.
(75) Yin, Q.; Tan, J. M.; Besson, C.; Geletii, Y. V.; Musaev, D. G.; Kuznetsov, A. E.; Luo, Z.; Hardcastle, K. I.; Hill, C. L. *Science* **2010**, *328*, 342–345.
(76) Brimblecombe, R.; Swiegers, G. F.; Dismukes, G. C.; Spiccia, L. *Angew. Chem., Int. Ed.* **2008**, *47*, 7335–7338.
(77) Dismukes, G. C.; Brimblecombe, R.; Felton, G. A. N.; Pryadun, R. S.; Sheats, J. E.; Spiccia, L.; Swiegers, G. F. *Acc. Chem. Res.* **2009**, *42*, 1935–1943.
(78) Li, G.; Sproviero, E. M.; Iii, R. C. S.; Iguchi, N.; Blakemore, J. D.; Crabtree, R. H.; Brudvig, G. W.; Batista, V. S. *Energy Environ. Sci.* **2009**, *2*, 230–238.
(79) Magnuson, A.; Anderlund, M.; Johansson, O.; Lindblad, P.; Lomoth, R.; Polivka, T.; Ott, S.; Stensjö, K.; Styring, S.; Sundström, V.; Hammarström, L. *Acc. Chem. Res.* **2009**, *42*, 1899–1909.
(80) Brimblecombe, R.; Koo, A.; Dismukes, G. C.; Swiegers, G. F.; Spiccia, L. *J. Am. Chem. Soc.* **2010**, *132*, 2892–2894.
(81) Dincă, M.; Surendranath, Y.; Nocera, D. G. *Proc. Natl. Acad. Sci. U. S. A.* **2010**, *107*, 10337–10341.
(82) Kopidakis, N.; Schiff, E. A.; Park, N. G.; van de Lagemaat, J.; Frank, A. J. *J. Phys. Chem. B* **2000**, *104*, 3930–3936.
(83) Nelson, J.; Chandler, R. E. *Coord. Chem. Rev.* **2004**, *248*, 1181–1194.
(84) Nelson, J.; Haque, S. A.; Klug, D. R.; Durrant, J. R. *Phys. Rev. B* **2001**, *63*, 205321.
(85) Bonhote, P.; Moser, J. E.; Humphry-Baker, R.; Vlachopoulos, N.; Zakeeruddin, S. M.; Walder, L.; Grätzel, M. *J. Am. Chem. Soc.* **1999**, *121*, 1324–1336.